Diffractive mirrors for neutral-atom matter-wave optics

Lee Yeong Kim,‡[a] Do Won Kang,‡[b], Sanghwan Park,[c], Seongyeop Lim,[c], Jangwoo Kim,[d], Wieland Schöllkopf,[e] and Bum Suk Zhao*[a,b]

Commercial gratings

Modern diffraction gratings are traditionally made using a ruling engine and a diamond stylus to burnish grooves or holographically using interference fringes produced by the intersection of two laser beams. We investigate four blazed gratings purchased from Newport: three plane-ruled gratings and one holographic grating. The two types of gratings consist of parallel edges as sketched in Fig. 1(a), which allows them to work as a reflection element. The periods d of the former are 20 μm, 3.3 μm, and 417 nm, while the latter has a period of 417 nm. The range of grating periods is selected to cover almost all commercially available grating. Their nominal blaze angles γ, i.e., the angle between the grating normal and the facet normal, are 0.8°, 6.5°, and 16.8° for the gratings of $d = 20$ μm, 3.3 μm, and 417 nm, respectively. Each grating has a thickness of 6 mm and a surface area of 50×50 mm^2. Each structure is patterned on a thin coating of evaporated aluminum on a glass substrate. We characterized the microscale structures of the grating edges with atomic force microscopy (AFM) and the macroscale radius of curvature of the overall gratings with interferometry, as detailed in the following paragraphs.

Microscale grating edge characterization

We characterized the edges of the two gratings with $d = 417$ nm by means of atomic force microscopy (AFM). Images were collected using a Dimension ICON AFM (Bruker) in tapping mode. We used conductive cantilever tips (PR-T300, Probes) with a resonance frequency of 325 kHz and a spring constant of $k = 40$ N/m. The tip-to-substrate distance was 30 nm, the drive amplitude was 127 mV, and the scan rate was between 0.3 and 1 Hz.

Figs. S1(a) and S1(b) [S1(c) and S1(d)] show 2D (3D) AFM images of the plane-ruled and holographic gratings, respectively. The scan dimensions of the selected areas are 2.5×2.5 μm^2. Along each row of a given y, we determined the local height maxima $h_{\max}$ at $(x_{\max}, y)$ for six grating grooves. The thick solid lines in Figs. S1(a, b) and S1(c, d) depict $x_{\max}(y)$ and $h_{\max}(x_{\max}, y)$, respectively. Then, $\Delta h_{\max}$ and $\Delta x_{\max}$, which are the standard deviations of $h_{\max}$ and $x_{\max}$, respectively, were evaluated for each groove. $\langle \Delta h_{\max} \rangle$ and $\langle \Delta x_{\max} \rangle$, which are the average values of $\Delta h_{\max}$ and $\Delta x_{\max}$ over the six grooves, represent the edge height roughness and the irregularity of the grating period, respectively.

The holographic grating has a better edge quality than the plane-ruled grating. In particular, the edges of the former are straighter than those of the latter. The $\langle \Delta h_{\max} \rangle$ and $\langle \Delta x_{\max} \rangle$ for the plane-ruled grating are 10 ± 2 nm and 19 ± 5 nm, respectively, which are larger than those for the holographic grating, 4.8 ± 0.5 nm and 15 ± 2 nm. Here, the uncertainty values are the standard deviations of the corresponding six datasets. The smaller $\langle \Delta h_{\max} \rangle$ and $\langle \Delta x_{\max} \rangle$ are, the straighter the grating edges are.

Macroscale radius of curvature of the gratings

Next, we evaluated the in-plane radius of curvature r of the grating. The reciprocal of r indicates the deviation degree of a curve from a straight line. The macroscale height function $H_{2D}(x, y)$ of the grating surface was measured using a Fizeau-type interferometer (Verifire, Zygo). The results are shown in Figs. S2(a) and S2(b). In these images, a single pixel corresponds to 50×50 μm^2, which covers 120 grooves in the 417-nm-period gratings. This resolution does not allow the detailed grating structure to be observed, so the obtained image represents the macroscopic topography. For an area on the surface of width W_x and height W_y [represented by the dotted square in Fig. S2(a)], we fit the profile $H(x; y)$ averaged along the y axis within W_y to a quadratic polynomial curve $H_{\text{fit}}(x; y) = ax^2 + bx + c$ considering the shape of $H(x; y)$. The center of the area is $(0, y)$. Since the part of the grating impacted by the incident beam is the projection of the incidence beam profile just after the Slit 2 on the grating, its width along the x-axis decreases with the incidence angle, but its height doesn't change. Therefore, we vary W_x from 50 to 20 mm and set W_y to 1 mm. In Figs. S2(c) and S2(d), the thick gray curve represents $H(x; y)$ for $y = 10$ mm, while the blue and red dashed curves depict H_{fit} for $W_x = 20$ and 40 mm, respectively. The chosen y value explains the experimental results well (see the next paragraph). It is known that $r = [1 + y'(x)^2]^{3/2}/|y''(x)|$ at (x, y) for a curve $y = f(x)$. For the fitted curves, therefore,

$$r = \frac{[1 + (\frac{dH_{\text{fit}}}{dx})^2]^{3/2}}{|\frac{d^2 H_{\text{fit}}}{dx^2}|} . \quad (1)$$

The r values of the two gratings are plotted as functions of the y position in Figs. S2(e) and S2(f) for W_x values ranging from 20 to 50 mm. In this evaluation, a positive value indicates a convex shape.

* Corresponding author
[a] Department of Physics, Ulsan National Institute of Science and Technology (UNIST), Ulsan 44919, Korea. E-mail: zhao@unist.ac.kr
[b] Department of Chemistry, Ulsan National Institute of Science and Technology (UNIST), Ulsan 44919, Korea
[c] School of Energy and Chemical Engineering, Ulsan National Institute of Science and Technology (UNIST), Ulsan 44919, Korea.
[d] Pohang Accelerator Laboratory, POSTECH, Pohang, Gyeongbuk 37673, Korea.
[e] Fritz-Haber-Institut der Max-Planck-Gesellschaft, Faradayweg 4-6, 14195 Berlin, Germany. E-mail: wschoell@fhi-berlin.mpg.de
‡ L. Y. K. and D. W. K. contributed equally to this work.

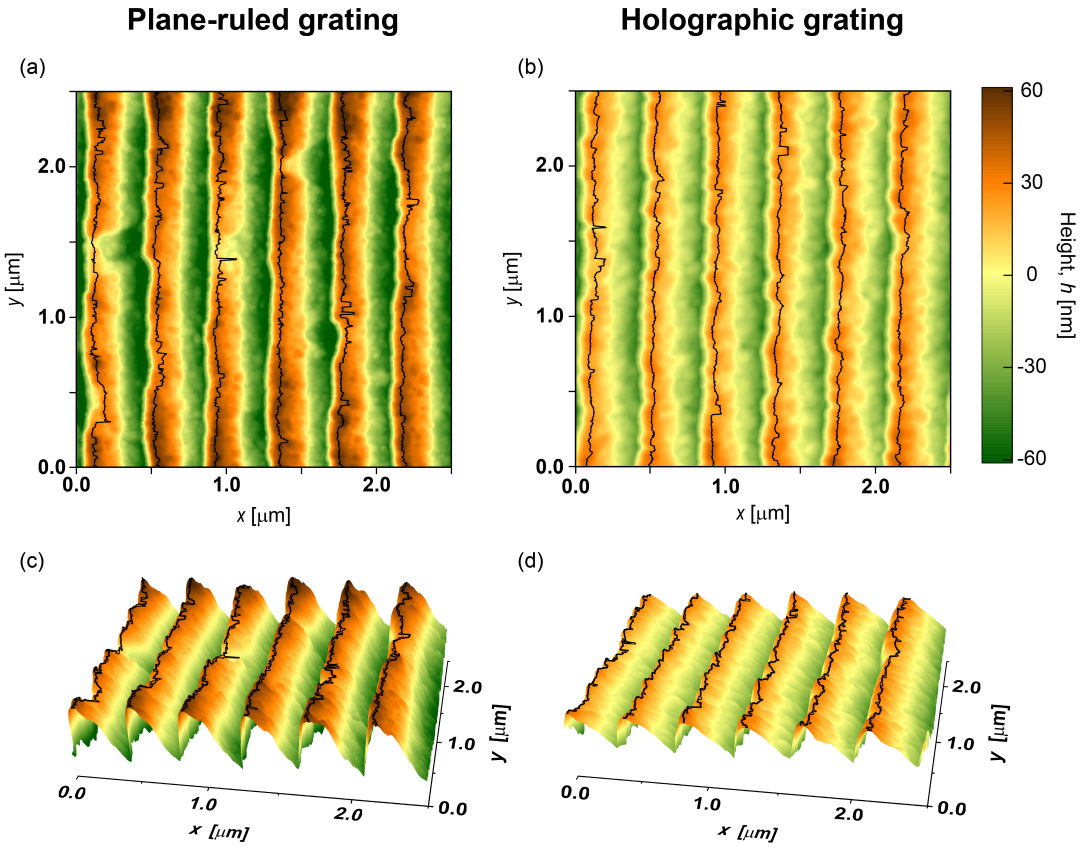

Fig. S1 Atomic force microscopy (AFM) images of the plane-ruled grating (first column) and the holographic grating (second column) with $d = 417$ nm. (a, b) 2D topography images. (c, d) 3D views. The three-dimensional black curves in the 3D graphs represent the local height maxima at given y values: $h_{\max}(x_{\max}, y)$. Here, $x_{\max}$ are the x positions at which the maxima occur, which are indicated by the two-dimensional black curves in the 2D graphs.

The results of this analysis show that the plane-ruled grating is flatter than the holographic grating and that their radii of curvature vary spatially. The $r = 480$ m value used in the width calculation in Fig. 3(b) in the main text [horizontal blue line in Fig. S2(f)] is close to the average value of r for different W_x values at $y = 10$ mm.

Experimental setup

The experimental configuration used in this study is similar to that used in our previous experiments, with the only difference being how the gratings are mounted [1,2]. Here, we use an in-plane mount in which the incident and scattered beams are in the scattering (or sagittal) plane, while we used an out-of-plane (conical) mount in our earlier work. The new arrangement makes good use of grating edges as opposed to the previous one, which uses grating facets to reflect atoms. In the apparatus, schematically illustrated in Fig. 1(b), a helium beam composed of He atoms and small clusters is formed by free-jet expansion of pure He gas through a 5-μm-diameter orifice into vacuum. The stagnation temperature and pressure, T_0 and P_0, indicate the conditions of the gas before the expansion. At $T_0 = 9.0$ K, we set P_0 to 0.5 and 2 bar for the atom and cluster experiments, respectively. As the gas enters the vacuum chamber, adiabatic expansion rapidly cools the gas to a temperature on the order of 1 mK, which allows some weakly bound dimers and trimers to form at the higher P_0 of 2 bar. The mean beam velocity of 305 m/s corresponds to the de Broglie wavelengths (λ) of He, He_2, and He_3 of 327, 164, and 109 pm, respectively. The beam is collimated by two 20-μm wide slits (Slit 1 and Slit 2) separated by 100 cm and scatters from the blazed grating at grazing incidence angles below 15 mrad. Here, the incidence angle θ_{in} and the detection angle θ are measured with respect to the grating surface plane as indicated in the inset of Fig. 1(b).

Data anaysis

We obtain spectra of the incident and specularly reflected beams at a range of detector angles θ_{det}, as depicted by the black and red solid lines in Fig. 1(c), respectively. The detector angles are set by precisely rotating the homemade mass spectrometer, which consists of an entrance slit (Slit 3), an electron impact ionizer, a magnet, and an ion detector. We obtain the former with the grating removed from the beam path and the latter with the holo-

graphic grating with $d = 0.417$ μm at $\theta_{\rm in} = 0.82 \pm 0.02$ mrad. By fitting the incident (or reflected) spectrum with a Gaussian function, we determine the peak area $A_{\rm in}$ (or A), full width at half maximum (FWHM) $w_{\rm in}$ (or w), and center position $\theta_{{\rm in},c}$ (or θ_c) of each peak. As shown in the graph, we set $\theta_{{\rm in},c} = 0$. Then, $\theta_{\rm in} = \theta_c/2$, and $\theta = \theta_{\rm det} - \theta_{\rm in}$. The reflected spectrum with a non-Gaussian shape shown in the graph is fit with multiple Gaussian functions whose centers are weight-averaged to obtain θ_c. The ratio $A/A_{\rm in}$ indicates the measured reflectivity of the surface at a given condition. For small incidence angles of $\theta_{\rm in} < 1$ mrad, we corrected the reflectivity with $A/(A_{\rm in} - 2A_{\rm in,wing})$ since only part of the incident beam hits the grating surface at these small incidence angles. Here, we assume that the incident beam hits the center of the grating, and $A_{\rm in,wing}$ is the area of a direct beam passing by one side of the grating, as depicted by the pink shadow in Fig. 1(c).

Notes and references

1 B. S. Zhao, G. Meijer and W. Schöllkopf, *Science*, 2011, **331**, 892–894.

2 B. S. Zhao, W. Zhang and W. Schöllkopf, *Sci. Adv.*, 2016, **2**, e1500901.

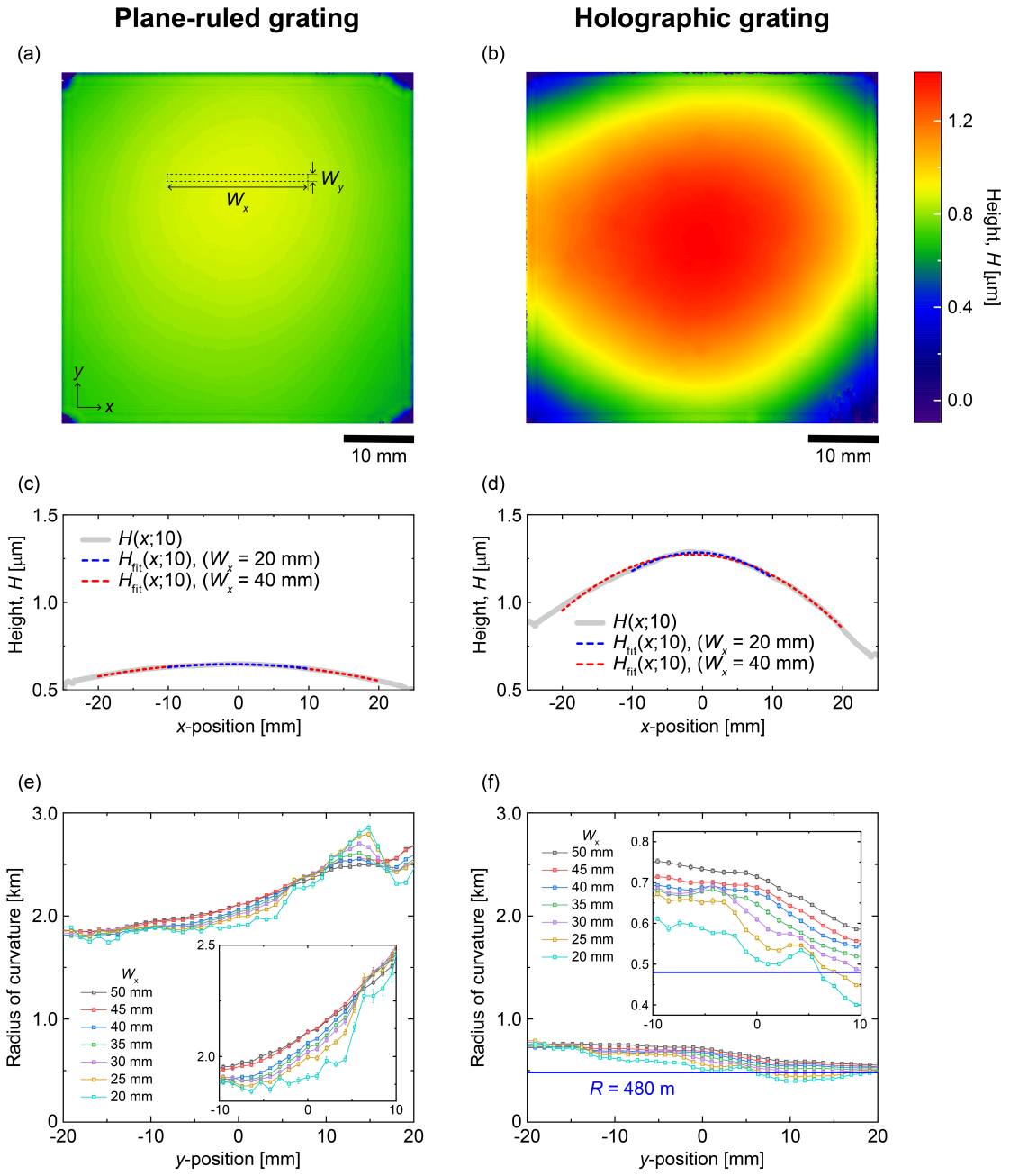

Fig. S2 Comparison between the macroscopic curvatures of the plane-ruled grating (first column) and the holographic grating (second column) with $d = 417$ nm. (a, b) Surface heights of the two gratings, $H_{2D}(x,y)$, measured by means of interferometry. The center of each two-dimensional graph, namely, the grating center, corresponds to the origin with coordinates $(x = 0, y = 0)$. (c, d) Surface height profiles along the x-axis at $y = 10$ mm, $H(x;y)$, and the curves fitted to the data, $H_{fit}(x;y)$. $H(x;y)$ is an average of $H_{2D}(x,y)$ over $y - W_y/2 < y < y + W_y/2$ with $W_y = 1$ mm. The measured profiles are depicted with thick gray lines, while the truncated blue and red dashed lines represent $H_{fit}(x;y)$ for $W_x = 20$ and 40 mm, respectively. (e, f) Radii of curvature of the two gratings for different W_x values as a function of y. The magnified graphs in the insets are the data associated with the vertical centers of two gratings.